THE EUROPEAN
PHYSICAL JOURNAL
SPECIAL TOPICS

Regular Article

Generalized Navier-Stokes equations for active suspensions

J. Słomka[a] and J. Dunkel[b]

Department of Mathematics, Massachusetts Institute of Technology, 77 Massachusetts Avenue E17, Cambridge, MA 02139-4307, USA

Abstract. We discuss a minimal generalization of the incompressible Navier-Stokes equations to describe the complex steady-state dynamics of solvent flow in an active suspension. To account phenomenologically for the presence of an active component driving the ambient fluid flow, we postulate a generic nonlocal extension of the stress-tensor, conceptually similar to those recently introduced in granular flows. Stability and spectral properties of the resulting hydrodynamic model are studied both analytically and numerically for the two-dimensional (2D) case with periodic boundary conditions. Future generalizations of this theory could be useful for quantifying the shear properties of active suspensions.

1 Introduction

An active suspension [1–7] is, roughly speaking, a passive fluid medium that contains at least one 'micro-swimmer' species capable of converting chemical into kinetic energy. If the swimmer concentration is sufficiently high, their collective dynamics can induce rich non-equilibrium flow patterns in the ambient fluid [8–16], thereby causing significant changes in the transport properties [17–20] and rheological response [21–24] of the solvent medium. An intriguing, seemingly generic feature of dense active suspensions is the emergence of a characteristic topological defect or vortex distance [5–7,12,25,26], thought to arise from the competition between self-propulsion, steric and hydrodynamic interactions [27]. Although the microscopic origins of such dynamical length-scale selection mechanisms are not yet fully understood, their experimentally confirmed presence [5–7,12,25] suggests that one can effectively describe active suspensions in terms of "non-local" higher-than-second-order partial differential equations (PDEs) [28], in analogy with well-established continuum theories of pattern formation in elastic materials [29], granular media [30] and convection phenomena [31].

Indeed, recent experimental and theoretical studies [7,12] confirm that a fourth-order extension of the Toner-Tu theory [32,33] can reproduce, both qualitatively

[a] e-mail: jslomka@mit.edu
[b] e-mail: dunkel@mit.edu

and quantitatively, many of the main statistical features of dense bacterial suspensions. Specifically, these experiments [7,12] measured the mean *bacterial* velocity field $\boldsymbol{u}(t, \boldsymbol{x})$, which can be approximately decomposed in the form $\boldsymbol{u}(t, \boldsymbol{x}) \simeq \boldsymbol{v}(t, \boldsymbol{x}) + v_0 \boldsymbol{P}(t, \boldsymbol{x})$, where $\boldsymbol{v}(t, \boldsymbol{x})$ is the underlying *solvent* velocity field and $\boldsymbol{P}(t, \boldsymbol{x})$ denotes the local mean orientation of the bacteria. The parameter v_0 is the typical bacterial self-swimming speed *relative to the solvent flow* (in general, v_0 is also a fluctuating quantity). The bacterial velocity data $\{\boldsymbol{u}\}$, obtained by standard PIV methods [2,5,8], were found to agree well with predictions of the incompressible fourth-order theory [7,12]

$$\nabla \cdot \boldsymbol{u} = 0 \tag{1a}$$
$$(\partial_t + \lambda_0 \boldsymbol{u} \cdot \nabla)\boldsymbol{u} = -\nabla(p - \lambda_1 \boldsymbol{u}^2) - \beta(\boldsymbol{u}^2 - u_0^2)\boldsymbol{u} + G_0 \nabla^2 \boldsymbol{u} - G_2 (\nabla^2)^2 \boldsymbol{u}, \tag{1b}$$

where the pressure $p(t, \boldsymbol{x})$ is the Lagrange multiplier for the incompressibility (bacterial mass conservation) constraint (1a). The parameter λ_0 describes nematic advection and λ_1 an active pressure contribution [28] that can be absorbed into a redefined pressure $p' = p - \lambda_1 \boldsymbol{u}^2$. The (β, u_0)-terms correspond to a quartic Landau-type velocity potential [33–35] and account for the formation of locally aligned bacterial jets [2]. The nonlocal (G_0, G_2)-terms encode passive and active stresses due to hydrodynamic and steric interactions, and determine the characteristic vortex size $\Lambda_\Gamma \simeq 2\pi\sqrt{G_2/(-G_0)}$ in the model when $G_2 > 0$ and $G_0 < 0$. Conceptually, Eqs. (1) extend the incompressible Toner-Tu theory [33–35] through the additional Swift-Hohenberg-type [31] instability that arises for $G_0 < 0$. A similar linear instability mechanism was recently derived by Großmann et al. [36] who considered a self-propelled particle model with velocity-dependent interaction. With regard to our subsequent discussion, it is important to note that Eqs. (1), which are defined in the rest-frame of the microfluidic channel confining the suspensions, are non-conservative due to the aligning β-term, reflecting the fact that the self-swimming field $v_0 \boldsymbol{P}$ is *not* a conserved quantity (just as in the classical Toner-Tu model [32,33]).

Although Eqs. (1) give satisfactory predictions for the *bacterial* velocity field $\boldsymbol{u}(t, \boldsymbol{x})$ in a stationary setting [7,12], they are of limited use with regard to shear experiments, which typically measure the response of the *solvent* flow in the presence of moving boundaries. Aiming to develop a simplified phenomenological framework for the future mathematical description of rheological measurements [21,22], we will focus here on the complementary problem of constructing effective models for the solvent velocity field $\boldsymbol{v}(t, \boldsymbol{x})$. Specifically, we are interested in identifying a minimal extension of the Navier-Stokes (NS) equations that reproduces qualitatively the experimentally observed, turbulent steady-state tracer dynamics in active suspensions [7]. In contrast to traditional approaches that build on explicit couplings between solvent flow and additional orientational order-parameter fields [9–11,15,24,37], we investigate here analytically and numerically higher-order *ad hoc* closure conditions for the stress tensor. Despite some technical differences, our approach shares conceptual similarities with the recently proposed, effectively non-local constitutive relations that have led to promising progress in the quantitative understanding of granular flows [38].

2 Generalized Navier-Stokes (NS) model

We focus on a coarse-grained model of active micro-swimmer suspensions, assuming that a single velocity field, $\boldsymbol{v}(t, \boldsymbol{x})$, describes the solvent flow on scales several times larger than an individual micro-swimmer. Considering incompressible solvent flow,

we postulate that the dynamics of $\boldsymbol{v}(t, \boldsymbol{x})$ is governed by the mass and momentum conservation laws

$$0 = \nabla \cdot \boldsymbol{v}, \tag{2a}$$

$$\partial_t \boldsymbol{v} + (\boldsymbol{v} \cdot \nabla)\boldsymbol{v} = -\nabla p + \nabla \cdot \boldsymbol{\sigma}, \tag{2b}$$

with scalar pressure $p(t, \boldsymbol{x})$ and symmetric stress tensor $\boldsymbol{\sigma}(t, \boldsymbol{x})$. Equation (2) implicitly assumes that the suspension has reached a (possibly turbulent) quasi-equilibrium state, in which the net momentum transfer between microswimmers and fluid becomes negligible. This restriction is consistent with the standard assumption that active filaments or microorganisms can be regarded as force-free [39–42] and torque-free [43] swimmers, which drive solvent flow by creating a stress field $\boldsymbol{\sigma}$.

Instead of constructing $\boldsymbol{\sigma}$ from orientational order-parameter fields [9–11,15,24, 37], we hypothesize that the steady-state stress generated by the micro-swimmers can be captured through a generic closed-form ansatz

$$\boldsymbol{\sigma} = \boldsymbol{\Sigma}(\nabla, \boldsymbol{v}). \tag{3}$$

In this paper, we will focus on a representative of the class of isotropic traceless tensors[1]

$$\boldsymbol{\Sigma}(\nabla, \boldsymbol{v}) = f(\nabla^2) \left[(\nabla \boldsymbol{v}) + (\nabla \boldsymbol{v})^\top \right], \tag{4}$$

where ∇^2 is the Laplace operator, and the scalar function $f(\cdot)$ quantifies the swimmers-solvent coupling. The symmetric ansatz (4) ensures that there is no net contribution to angular momentum from internal stresses, reflecting the assumption that the swimmers are torque-free [43].

Intuitively, Eq. (4) can be thought of as a leading-order stress contribution linear in $\boldsymbol{v}$, arising from a truncated gradient expansion of an integral kernel representation of the 'full' stress tensor $\boldsymbol{\sigma}$, similar to a Kramers-Moyal expansion [44]. In particular, for a constant function $f(\nabla^2) \equiv \Gamma_0$, corresponding to a passive isotropic fluid, Eqs. (2) reduce to the standard Navier-Stokes equations. In this limit case, Γ_0 is the usual kinematic viscosity and depends on the volume filling fraction of (non-motile) micro-swimmers.

In the remainder, we will restrict the discussion to symmetric second-order polynomials

$$f(\nabla^2) = \Gamma_0 - \Gamma_2(\nabla^2) + \Gamma_4(\nabla^2)^2. \tag{5}$$

The constants Γ_0 and Γ_4 are assumed to be positive to ensure asymptotic stability, whereas the parameter Γ_2 may have either sign. Nontrivial steady-state flow structures emerge for negative values $\Gamma_2 < 0$. Inserting Eqs. (4) and (5) into Eqs. (2), we obtain the hydrodynamic equations

$$0 = \nabla \cdot \boldsymbol{v}, \tag{6a}$$

$$\partial_t \boldsymbol{v} + (\boldsymbol{v} \cdot \nabla)\boldsymbol{v} = -\nabla p + \Gamma_0 \nabla^2 \boldsymbol{v} - \Gamma_2 \nabla^4 \boldsymbol{v} + \Gamma_4 \nabla^6 \boldsymbol{v}, \tag{6b}$$

where $\nabla^{2n} \equiv (\nabla^2)^n$ from now on. Below, we analyze the generalized NS equations (6) on a 2D square domain. Since we aim to understand their bulk properties, we adopt periodic boundary conditions throughout.

---

[1] More generally, one could also consider additional quasi-nematic stress contributions $\propto \boldsymbol{vv} - \boldsymbol{I}|\boldsymbol{v}|^2/d$, where $\boldsymbol{I}$ is the d-dimensional identity tensor. Such terms would effectively rescale the advective derivative and add a kinetic pressure contribution.

3 Analytical results

To obtain some intuition about the generalized NS model (6), we first note that its linear part supports a stationary vortex lattice of period $\sim \sqrt{\Gamma_4/(-\Gamma_2)}$, when Γ_2 is negative. This follows from the fact that

$$\left(\Gamma_0\nabla^2 - \Gamma_2\nabla^4 + \Gamma_4\nabla^6\right)e^{i\boldsymbol{k}\cdot\boldsymbol{x}} = 0 \tag{7}$$

if $k = |\boldsymbol{k}|$ is one of the roots of $\Gamma_0 + \Gamma_2 k^2 + \Gamma_4 k^4 = 0$, with real positive roots existing only when $\Gamma_2 < 0$. Furthermore, since the nonlinear advective terms on the lhs. of Eq. (6b) will generally lead to mixing, one can expect to find parameters such that Eqs. (6) produce turbulent mesoscale patterns similar to those observed in experiments [5,7,12].

To perform a more detailed stability analysis, we focus on a periodic square domain $\Omega = [-L/2, L/2]^2$ and rescale Eqs. (6) by introducing dimensionless quantities

$$\boldsymbol{x} \to \frac{2\pi}{L}\boldsymbol{x}, \quad t \to \frac{(2\pi)^2\Gamma_0}{L^2}t, \quad \boldsymbol{v} \to \frac{L}{2\pi\Gamma_0}\boldsymbol{v}, \quad p \to \frac{L^2}{(2\pi)^2\Gamma_0^2}p, \quad \boldsymbol{k} \to \frac{L}{2\pi}\boldsymbol{k}. \tag{8}$$

One then finds that the dynamics of the model is characterized by the two dimensionless groups

$$\gamma = \frac{\Gamma_0\Gamma_4}{\Gamma_2^2}, \qquad \gamma_2 = \frac{(2\pi)^2\Gamma_2}{L^2\Gamma_0}, \tag{9}$$

and the rescaled Eqs. (6) take the form

$$\nabla \cdot \boldsymbol{v} = 0 \tag{10a}$$
$$\partial_t\boldsymbol{v} + (\boldsymbol{v}\cdot\nabla)\boldsymbol{v} = -\nabla p + \nabla^2\boldsymbol{v} - \gamma_2\nabla^4\boldsymbol{v} + \gamma\gamma_2^2\nabla^6\boldsymbol{v}. \tag{10b}$$

To ensure stability at short wavelengths, γ must be always positive. Nontrivial flow structures require $\gamma_2 < 0$. We expect that there is a region in the (γ, γ_2)-parameter space that supports a quasi-chaotic steady-state dynamics characterized by the creation and annihilation of vortices.

To estimate this parameter region, we investigate how the total kinetic energy, $E(t) = \frac{1}{2}\int_\Omega d\boldsymbol{x}\,|\boldsymbol{v}|^2$, varies with time. From the equations of motion with periodic boundary conditions, one finds

$$\begin{aligned}
\dot{E}(t) &= \int_\Omega d\boldsymbol{x}\,\boldsymbol{v}\cdot\partial_t\boldsymbol{v} \\
&= \int_\Omega d\boldsymbol{x}\left[-\nabla\cdot\left(\frac{1}{2}|\boldsymbol{v}|^2\boldsymbol{v} + p\boldsymbol{v}\right) + \boldsymbol{v}\cdot(\nabla^2\boldsymbol{v} - \gamma_2\nabla^4\boldsymbol{v} + \gamma\gamma_2^2\nabla^6\boldsymbol{v})\right] \\
&= \int_\Omega d\boldsymbol{x}\,\boldsymbol{v}\cdot\left(\nabla^2\boldsymbol{v} - \gamma_2\nabla^4\boldsymbol{v} + \gamma\gamma_2^2\nabla^6\boldsymbol{v}\right). \tag{11}
\end{aligned}$$

We next insert the Fourier series for the velocity, $\boldsymbol{v}(t,\boldsymbol{x}) = \mathcal{F}^{-1}(\hat{\boldsymbol{v}}) \equiv \sum_{\boldsymbol{k}} e^{i\boldsymbol{k}\cdot\boldsymbol{x}}\hat{\boldsymbol{v}}(t,\boldsymbol{k})$, where $\boldsymbol{k} \in \mathbb{Z}^2$, to obtain

$$\dot{E}(t) = -(2\pi)^2 \sum_{\boldsymbol{k}} k^2\big(1 + \gamma_2 k^2 + \gamma\gamma_2^2 k^4\big)|\hat{v}(t,\boldsymbol{k})|^2. \tag{12}$$

The first and the third term in the brackets are always positive, and therefore dissipate energy. If $\gamma_2 > 0$ holds, then $\dot{E} < 0$ always; in this case, any solvent flow in the system is rapidly damped out. More interestingly, however, when $\gamma_2 < 0$, the active component pumps energy into the flow. We may then ask if, at least for some region in the (γ, γ_2)-plane, the energy input and the energy dissipation can balance each other. If such a steady-state exists, then the total system energy should fluctuate about a constant mean value. More formally, we expect in this case that the mean energy change vanishes,

$$\langle \dot{E} \rangle_{\Delta, T} \equiv \lim_{\Delta \to \infty} \lim_{T \to \infty} \frac{1}{\Delta} \int_T^{T+\Delta} \dot{E}(t) dt \to 0, \tag{13a}$$

and that the time-averaged Fourier coefficients become stationary and isotropic,

$$\langle |\hat{\boldsymbol{v}}(t, \boldsymbol{k})|^2 \rangle_{\Delta, T} \to \langle |\hat{\boldsymbol{v}}(k)|^2 \rangle. \tag{13b}$$

Provided that the steady-state is attainable, we have the following energy balance equation

$$\sum_k k^2 \left(1 + \gamma_2 k^2 + \gamma \gamma_2^2 k^4\right) \mathcal{E}(k) = 0, \tag{14a}$$

where the energy spectrum, $\mathcal{E}(k)$, is defined as [45]

$$\left\langle \frac{1}{2} \int_\Omega d\boldsymbol{x} \, |\boldsymbol{v}|^2 \right\rangle_{\Delta, T} = \sum_k \mathcal{E}(k), \tag{14b}$$

yielding

$$\mathcal{E}(k) = \frac{(2\pi)^2}{2} \sum_{\boldsymbol{k}': |\boldsymbol{k}'| = k} \langle |\hat{\boldsymbol{v}}(k')|^2 \rangle. \tag{15}$$

Building on the above considerations, we can now analytically estimate the part of the (γ, γ_2)-parameter plane where a steady-state can be reached. Neglecting pressure, the linearized version of Eq. (10b) reads

$$\partial_t \boldsymbol{v} = \nabla^2 \boldsymbol{v} - \gamma_2 \nabla^4 \boldsymbol{v} + \gamma \gamma_2^2 \nabla^6 \boldsymbol{v}. \tag{16}$$

Using the Fourier series for $\boldsymbol{v}$ as before, this is equivalent to

$$\partial_t \hat{\boldsymbol{v}}(t, \boldsymbol{k}) = \Lambda(k) \, \hat{\boldsymbol{v}}(t, \boldsymbol{k}), \tag{17a}$$

where

$$\begin{aligned} \Lambda(k) &= -k^2(1 + \gamma_2 k^2 + \gamma \gamma_2^2 k^4) \\ &= -\gamma \gamma_2^2 k^2 (k^2 - k_-^2)(k^2 - k_+^2). \end{aligned} \tag{17b}$$

The range of physically reasonable zeros $k_\pm$ can be inferred from stability considerations as follows:

Fourier modes may become unstable if the micro-swimmers inject a sufficiently large amount of energy into the system. In the linearized model, such supercritical energy injection leads to divergence at an exponential rate. However, the advective
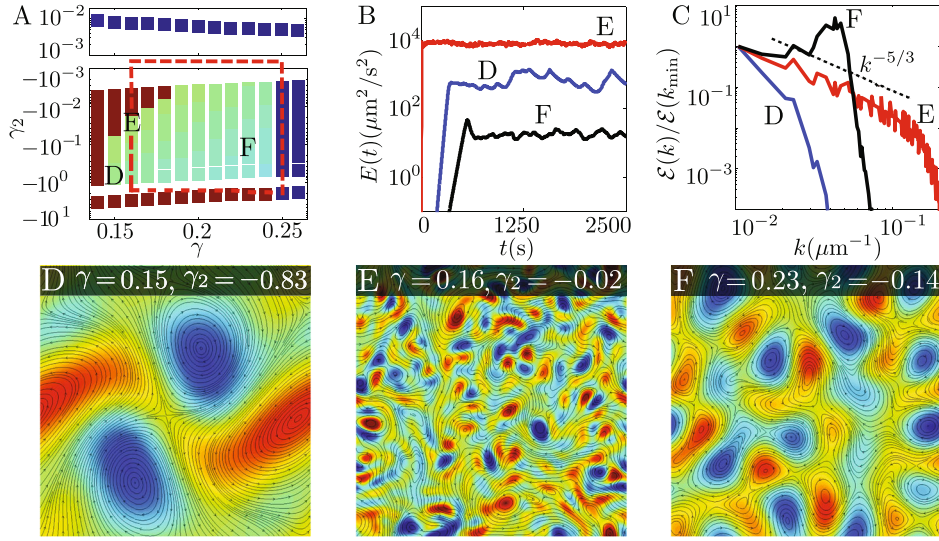
Fig. 1. Simulation results for the rescaled generalized Navier-Stokes model defined in Eqs. (10). A) Numerical stability analysis in the (γ, γ_2)-parameter plane. Nontrivial energetically stable steady-state solutions exist in the green region (labels D, E and F correspond to snapshots shown in panels D-F). The numerical results agree well with the analytically predicted region of flow structure formation (red dashed lines) obtained in Sect. 3. In the purely dissipative regime (dark blue), the system converges to the zero-flow solution. The truncated model becomes unstable (brown region) when the dissipation is not able to balance the energy input. B, C) Kinetic energy as a function of time, $E(t)$, and corresponding normalized energy spectra, $\mathcal{E}(k)$, for the three parameter choices in the bottom row. D–F) Snapshots of the steady-state flow stream lines for simulations with periodic boundary conditions. The background color represents the associated vorticity fields $\omega = \nabla \wedge \boldsymbol{v}$, normalized by their maximal values. The domain size is $L \times L$, with $L = 600 \,\mu\mathrm{m}$ in physical units.

term in the full nonlinear system mixes different modes, facilitating energy dissipation through the decaying modes. The stability of a given mode is determined by the sign of $\Lambda(k)$. To observe non-trivial flow structures, we require $\Lambda(k) > 0$ for some $k > 0$, implying that $\gamma_2 < 0$ and $\gamma < 1/4$, because otherwise $(1 + \gamma_2 k^2 + \gamma \gamma_2^2 k^4) > 0$ and, hence, no real positive roots $k_\pm$ exist. Furthermore, its is plausible to assume that any realistic active system has a long-wavelength cut-off corresponding to the largest scale at which energy is collectively injected into the fluid, implying that the system should be dissipative in some vicinity of its lowest mode, $k = 1$. Otherwise, there is no room left for an inverse dissipative energy cascade and the energy could continuously accumulate at long wavelengths. We therefore demand $k_- > 1$, which implies that $\gamma_2 > \frac{1}{-2\gamma}(1 - \sqrt{1 - 4\gamma})$. Thus, all discrete $\boldsymbol{k}$-modes lying in the annular region $1 < k_- < k < k_+$ inject energy, whereas the complementary set of modes dissipates energy. For instance, if we adopt the simplifying assumption that, as in classical 2D turbulent flow, $\mathcal{E}(k)$ scales as $k^{-5/3}$ up to some cut-off mode, which we take to be the largest unstable mode, $k_+^2 = \frac{1}{-2\gamma\gamma_2}(1 + \sqrt{1 - 4\gamma})$, then, after approximating the sum by an integral, Eq. (14a) predicts the critical value of $\gamma = 0.16$. In summary, these considerations suggest that an energetically stable, nontrivial steady-state can be reached in the parameter range $0.16 < \gamma < 0.25$ and $0 > \gamma_2 > \frac{1}{-2\gamma}(1 - \sqrt{1 - 4\gamma})$. These simple estimates agree well with our numerical results, as shown in Fig. 1A.

4 Stream function formulation and numerical implementation

To solve Eqs. (10) numerically, it is convenient to reformulate the dynamical equations (10) in terms of a stream function. By means of the Helmholtz-Hodge decomposition [46], we can express the solvent flow field $\boldsymbol{v}$ as a sum of divergence-free, curl-free and harmonic components,

$$\boldsymbol{v} = \nabla\Phi + \nabla \wedge \Psi + \boldsymbol{V}, \tag{18}$$

for some scalar function $\Phi(t, \boldsymbol{x})$, pseudo-scalar function $\Psi(t, \boldsymbol{x})$ and a harmonic vector field $\boldsymbol{V}(t, \boldsymbol{x})$ satisfying $\nabla^2 \boldsymbol{V} = 0$. The $\wedge$-product is defined by $\nabla \wedge \Psi = (\epsilon_{ij}\partial_i\Psi)$ with ϵ_{ij} denoting the components of the 2D Levi-Civita tensor; similarly, for two 2D vectors $\boldsymbol{a} = (a_1, a_2)$ and $\boldsymbol{b} = (b_1, b_2)$, we have $\boldsymbol{a} \wedge \boldsymbol{b} = \epsilon_{ij}a_i b_j$. On periodic domains, harmonic functions are constant, so $\boldsymbol{V}$ is interpreted as the fluid center of mass velocity. We will always work in the center of mass frame, hence $\boldsymbol{V} = 0$ from now on. Similarly, Φ is also a constant since incompressibility implies that $\nabla^2\Phi = 0$, so that Φ is a harmonic function. Thus, Eq. (18) reduces to $\boldsymbol{v} = \nabla \wedge \Psi$.

To obtain the evolution equation for Ψ, we take the divergence and the curl of Eq. (10b), which gives

$$(\nabla\nabla\Psi) : (\nabla\nabla\Psi) - (\nabla^2\Psi)^2 = -\nabla^2 p, \tag{19a}$$

$$\partial_t(\nabla^2\Psi) + \nabla(\nabla^2\Psi) \wedge \nabla\Psi = \nabla^4\Psi - \gamma_2\nabla^6\Psi + \gamma\gamma_2^2\nabla^8\Psi. \tag{19b}$$

The main advantage of this reformulation lies in the fact that the stream function Ψ is now the only dynamical variable, as the pressure p can always be recovered from Ψ by solving the Poisson Eq. (19a).

The governing equation for the stream function, Eq. (19a), can be solved with standard spectral methods [47]. Using the Fourier series representation, the modes of Ψ evolve according to

$$\partial_t\hat{\Psi} + \mathcal{N} = -k^2(1 + \gamma k^2 + \gamma\gamma_2^2 k^4)\hat{\Psi}, \tag{20a}$$

where the nonlinear terms are abbreviated by

$$\mathcal{N} = k^{-2}\mathcal{F}\{\mathcal{F}^{-1}(i\boldsymbol{k}k^2\hat{\Psi}) \wedge \mathcal{F}^{-1}(i\boldsymbol{k}\hat{\Psi})\}. \tag{20b}$$

We integrated Eqs. (20) with a classical fourth-order Runge-Kutta scheme, and approximated $\mathcal{F}(\cdot)$ by a Discrete Fourier Transform (DFT). The nonlinear term $\mathcal{N}$ is evaluated by inverting the DFT, performing the multiplication in position space, and then applying the DFT again. The aliasing error generated in this procedure is removed at the expense of using a larger number of Fourier modes and zero-padding when necessary (see [47] for a detailed description of this method; in our simulations, we used a symmetric grid of 243×243 modes).

5 Results

We first investigated the stability of numerical solutions of Eqs. (10) on a periodic $L \times L$ square domain by performing systematic scan of the (γ, γ_2)-parameter plane, initializing each simulation run with small random stream function values. In agreement with our analytical considerations in Sect. 3, we found three qualitatively different asymptotic behaviors:

(i) For $\gamma_2 > 0$ or when γ becomes too large, the solvent dynamics is purely dissipative and approaches a stationary state of vanishing flow $\boldsymbol{v} \equiv 0$ (blue symbols in Fig. 1A).

(ii) For $\gamma_2 < 0$ and γ too small, the solutions become unstable, reflected by an exponential blow-up of the kinetic energy (brown symbols in Fig. 1A).

(iii) For $\gamma_2 < 0$ and moderate values of γ the system exhibits quasi-chaotic steady-state flow patterns (green symbols in Fig. 1A). The numerically estimated boundaries of this physically relevant domain agree well with the analytical estimates (red dashed lines) from Sect. 3.

Example snapshots of quantitatively different flow patterns for three parameter pairs (γ, γ_2) are shown in Fig. 1D–F. For all three parameter pairs, the kinetic energy approaches a constant mean value (Fig. 1B). As γ approaches the upper critical value 0.25, the corresponding energy spectra develop peaks near the linearly most unstable wave number, $k_* \sim -(2\gamma\gamma_2)^{-1}$ (black curve F in Fig. 1C). In position space, such peaks correspond to a characteristic vortex size $\sim k_*^{-1}$ (Fig. 1F). For comparison, the blue and red curves in Fig. 1B,C represent two opposite extremes at small values of γ exhibiting very large and small vortices, respectively (Fig. 1D,E). The vortex diameter in Fig. 1D approaches $\sim 1/2$ of the total system size L, corresponding to the second smallest k-mode in our simulations. Accordingly, this vortex length scale appears as a maximum at the lower boundary of the k-range (blue curve D in Fig. 1C). In the opposite limit, when the characteristic vortex size becomes very small (Fig. 1E), the spectrum is well approximated by a Kolmogorov scaling law $\mathcal{E}(k) \propto k^{-5/3}$ as typical of the upward cascade in classical 2D turbulence (red curve E in Fig. 1C). This supports the assumptions made in Sect. 3 to derive the left vertical red dashed line in Fig. 1A. Although this upward cascade "smears out" the spectrum at smaller wave numbers, a remnant of the characteristic vortex size remains visible as a kink at high wave-numbers (red curve E in Fig. 1C).

To relate the dimensionless parameters in our 2D simulations to physical relevant dimensional values, we may fix $\Gamma_0 = 10^2 \, \mu\text{m}^2/\text{s}$ and identify the box length with $L = 600 \, \mu\text{m}$. With these choices, the typical steady-state speeds are in the range of $1 \, \mu\text{m/s}$ to $100 \, \mu\text{m/s}$, as typical of passive tracer particles in dense bacterial suspensions [7].

Furthermore, we would still like to emphasize that the unstable regime (brown symbols in Fig. 1A) arises from the particular truncated polynomial ansatz in Eq. (5). Future quantitative comparison with experiments should focus on reconstructing better approximations of the function f or, more generally, $\boldsymbol{\sigma}$. Conversely, however, stability criteria provide useful physical constraints for effective models that can be utilized in parameter estimation procedures.

Although we restricted our numerical analysis to the 2D case, the generalized Navier-Stokes model defined in Sect. 2 remains valid in 3D. If one adopts the truncated polynomial ansatz (5), many qualitative flow characteristics are expected to persist in higher dimensions, but the partial Kolmogorov scaling regime is unlikely to be seen. This is due to the fact that, in classical 3D turbulence, a spectral decay $\propto k^{-5/3}$ is associated with a downward cascade towards larger k-modes (smaller wave-lengths), whereas in the polynomial model (6) the large-k dynamics is dominated by the k^6-damping term. To observe Kolmogorov scaling in the 3D generalized Navier-Stokes model, one would have to modify the stress tensor such that it exhibits asymptotically linear k-scaling at both small and large wave-numbers. This is achievable by postulating non-polynomial functions f in Eq. (4).

6 Summary

We proposed and analyzed a minimal generalization of the Navier-Stokes equation to describe the steady-state solvent flow in an active suspension. The main assumption

underlying this simple momentum-conserving model is that, on scales larger than the swimming cells or filaments, the complex fluid-swimmer interactions can be effectively captured by a generalized form of the stress energy tensor, which can be expanded in terms of higher-order differential operators. In this contribution, we focussed on a simple example, corresponding to a sixth-order PDE, that produces turbulent flow features that are qualitatively similar to those observed through passive tracer-particle tracking in recent experiments [7].

A future goal is to embed this class of models into a shear-flow setting as relevant to viscosity measurements [21,22]. This problem is conceptually and numerically nontrivial as appropriate boundary conditions need to be identified and implemented. Notwithstanding, such a phenomenological approach may help us to progress towards a sufficiently-general-yet-reasonably-simple framework for the classification of rheological observations in active suspensions. From a practical perspective, an interesting challenge will be to reconstruct an empirical form of the generalized stress-tensor $\boldsymbol{\sigma}$ from experimentally measured solvent flow data.

References

1. M.C. Marchetti, J.F. Joanny, S. Ramaswamy, T.B. Liverpool, J. Prost, M. Rao, R.A. Simha, Rev. Mod. Phys. **85**, 1143 (2013)
2. L.H. Cisneros, R. Cortez, C. Dombrowski, R.E. Goldstein, J.O. Kessler, Exp. Fluids **43**, 737 (2007)
3. H.P. Zhang, A. Be'er, E.L. Florin, H.L. Swinney, Proc. Natl. Acad. Sci. USA **107**, 13626 (2010)
4. V. Schaller, C. Weber, C. Semmrich, E. Frey, A.R. Bausch, Nature **467**, 73 (2010)
5. A. Sokolov, I.S. Aranson, Phys. Rev. Lett. **109**, 248109 (2012)
6. T. Sanchez, D.T.N. Chen, S.J. DeCamp, M. Heymann, Z. Dogic, Nature **491**, 431 (2012)
7. J. Dunkel, S. Heidenreich, K. Drescher, H.H. Wensink, M. Bär, R.E. Goldstein, Phys. Rev. Lett. **110**, 228102 (2013)
8. C. Dombrowski, L. Cisneros, S. Chatkaew, R.E. Goldstein, J.O. Kessler, Phys. Rev. Lett. **93**(9), 098103 (2004)
9. C.W. Wolgemuth, Biophys. J. **95**, 1564 (2008)
10. A. Baskaran, M.C. Marchetti, Proc. Natl. Acad. Sci. **106**, 15567 (2009)
11. D. Saintillan, M. Shelley, J. R. Soc. Interface **9**, 571 (2011)
12. H.H. Wensink, J. Dunkel, S. Heidenreich, K. Drescher, R.E. Goldstein, H. Löwen, J.M. Yeomans, Proc. Natl. Acad. Sci. USA **109**, 14308 (2012)
13. F.G. Woodhouse, R.E. Goldstein, Phys. Rev. Lett. **109**, 168105 (2012)
14. T. Brotto, J.B. Caussin, E. Lauga, D. Bartolo, Phys. Rev. Lett. **110**, 038101 (2013)
15. L. Giomi, M.J. Bowick, X. Ma, M.C. Marchetti, Phys. Rev. Lett. **110**, 228101 (2013)
16. A. Zöttl, H. Stark, Phys. Rev. Lett. **112**, 118101 (2014)
17. X.L. Wu, A. Libchaber, Phys. Rev. Lett. **84**, 3017 (2000)
18. K.C. Leptos, J.S. Guasto, J.P. Gollub, A.I. Pesci, R.E. Goldstein, Phys. Rev. Lett. **103**, 198103 (2009)
19. J. Dunkel, V.B. Putz, I.M. Zaid, J.M. Yeomans, Soft Matter **6**, 4268 (2010)
20. I.M. Zaid, J. Dunkel, J.M. Yeomans, J. R. Soc. Interface **8**, 1314 (2011)
21. A. Sokolov, I.S. Aranson, Phys. Rev. Lett. **103**(14), 148101 (2009)
22. S. Rafai, L. Jibuti, P. Peyla, Phys. Rev. Lett. **104**, 098102 (2010)
23. S.D. Ryan, B.M. Haines, L. Beryland, F. Ziebert, I.S. Aranson, Phys. Rev. E **83**, 050904(R) (2011)

24. G. Foffano, J.S. Lintuvuori, A.N.M. nd K. Stratford, M.E. Cates, D. Marenduzzo, Eur. Phys. J. E **35**, 98 (2012)
25. H. Wioland, F.G. Woodhouse, J. Dunkel, J.O. Kessler, R.E. Goldstein, Phys. Rev. Lett. **110**, 268102 (2013)
26. S.P. Thampi, R. Golestanian, J.M. Yeomans, Phys. Rev. Lett. **111**, 118101 (2013)
27. E. Lushi, H. Wioland, R.E. Goldstein, Proc. Natl. Acad. Sci. USA **111**, 9733 (2014)
28. J. Dunkel, S. Heidenreich, M. Bär, R.E. Goldstein, New J. Phys. **15**, 045016 (2013)
29. L.D. Landau, E.M. Lifshitz, *Theory of Elasticity* (Pergamon, London, 1959)
30. I.S. Aranson, L.S. Tsimring, Rev. Mod. Phys. **78**, 641 (2006)
31. J. Swift, P.C. Hohenberg, Phys. Rev. A **15**, 319 (1977)
32. J. Toner, Y. Tu, Phys. Rev. Lett. **75**, 4326 (1995)
33. J. Toner, Y. Tu, Phys. Rev. E **58**, 4828 (1998)
34. J. Toner, Y. Tu, S. Ramaswamy, Ann. Phys. **318**, 170 (2005)
35. S. Ramaswamy, Annu. Rev. Cond. Mat. Phys. **1**, 323 (2010)
36. R. Großmann, P. Romanczuk, M. Bär, L. Schimansky-Geier, Phys. Rev. Lett. **113**, 258104 (2014)
37. R.A. Simha, S. Ramaswamy, Phys. Rev. Lett. **89**, 058101 (2002)
38. D.L. Henann, K. Kamrin, Proc. Nat. Acad. Sci. **110**, 6730 (2013)
39. A. Najafi, R. Golestanian, Phys. Rev. E **69**, 062901 (2004)
40. C.M. Pooley, G.P. Alexander, J.M. Yeomans, Phys. Rev. Lett. **99**, 228103 (2007)
41. K. Drescher, J. Dunkel, L.H. Cisneros, S. Ganguly, R.E. Goldstein, Proc. Natl. Acad. Sci. USA **108**, 10940 (2011)
42. J.S. Guasto, K.A. Johnson, J.P. Gollub, Phys. Rev. Lett. **105**, 168102 (2010)
43. E. Lauga, T.R. Powers, Rep. Prog. Phys. **72**, 096601 (2009)
44. H. Risken, *The Fokker-Planck Equation: Methods of Solutions and Applications*, 2nd edn. (Springer, Berlin, 1996)
45. U. Frisch, *Turbulence* (Cambridge University Press, Cambridge, England, 2004)
46. R. Abraham, J. Marsden, T. Ratiu, *Manifolds, Tensor Analysis, and Applications*, Vol. 75 of *Applied Mathematical Sciences* (Springer, 1989)
47. C. Canuto, M. Hussaini, A. Quarteroni, T. Zang, *Spectral Methods in Fluid Dynamics* (Springer-Verlag, Berlin, 1987)